Structural Engineering and Mechanics, Vol. 15, No. 4 (2003) 451-462
DOI: http://dx.doi.org/10.12989/sem.2003.15.4.451

Modal control algorithm on optimal control of intelligent structure shape

Guo Feng Yao†, Su Huan Chen† and Wei Wang‡

Department of Mechanics, Nailing Campus, Jilin University, Changchun, 130025, P.R. China

(Received July 17, 2002, Accepted February 18, 2003)

Abstract. In this paper, a new block iterative algorithm is presented by using the special feature of the continuous Riccati equation in the optimal shape control. Because the real-time control require that the CPU time should be as short as possible, an appropriate modal control algorithm is sought. The computing cost is less than the one of the all state feedback control. A numerical example is given to illustrate the algorithm.

Key words: intelligent structure; optimal shape control; block iterative algorithm; modal control.

1. Introduction

Space structures, aircraft, and the like are required to be light in weight due to the high cost of transportation. Since they are also lightly damped, owing to the low internal damping of the materials used in their construction, the increased flexibility may allow large amplitude vibration and shape deformation, which may cause structural instability. These problems lead to a drastic reduction in accuracy and precision of operation. Thus, it is highly desirable to control excessive vibration and shape deformation and to stabilize the structure during operation (Atluri *et al.* 1988 and Meirovitch 1990).

This paper is concerned with thin piezoelectric layers which are coupled with conventional materials and used as distributed sensors and distributed actuators in an intelligent advanced structure design(Hwang *et al.* 1993, Im *et al.* 1989, Tzou *et al.* 1990 and Chen *et al.* 2001). One piezoelectric layer serves as a distributed sensor and the other layer serves as a distributed actuator. The direct effect is used in distributed sensing and the converse effect in distributed active vibration suppression and shape control of the advanced structure. Thus the sensing layer detects the oscillation of the distributed systems and the actuator controls the vibration or shape of the system.

Up to now, research in this area has been primarily focused on experimental and theoretical studies. In general, experimental models are limited by size, cost, and many other laboratory unknowns. Theoretical models can be more general, but analytical solutions are restricted to relatively simple geometries and boundary conditions. When the geometry and boundary conditions become relatively complicated, difficulties occur with both theoretical and experimental models.

† Professor
‡ Assistant Professor, Changchun University

Thus, the finite element development becomes very important in modeling and analysis of advanced flexible structures with integrated distributed piezoelectric sensors and/or actuators (Shi *et al*. 1990).

Before now, only beam elements (Hwang *et al.* 1993 and Im *et al*. 1989), plate elements and isoparametric hexahedron solid elements (Tzou *et al*. 1990) were developed. They don't suit to three-dimensional thin shell structure, for instance, a paraboloid antenna for controlling its shape and suppressing its oscillation. Therefore, Chen *et al*. (2001) presents an eight-node and forty-DOF isoparametric shell element (Guyan 1965 and Xie *et al*. 1981) in which the shear effects are considered, and a finite element formulation (Xie and He 1981, Zhang *et al.* 1986 and Zienkiewicz 1971) is presented for modeling the dynamic as well as static response of laminated shell structure containing distributed piezoelectric materials (PVDF) subjected to both mechanical and electrical load.

By using the feature of Riccati equation in the optimal shape control, a new block iterative algorithm is given. It can save the memory and reduce the CPU time. If the order of the finite element equation is very large (for example, more than 1000), all methods cannot ensure the real-time control. In order to solve the problem, the modal control algorithm is presented to ensure both the real-time control and precision of the shape control. Finally, a numerical example is given to illustrate the modal control algorithm.

2. The Riccati equation in the optimal shape control

The finite element equation (Ahmad *et al*. 1970 and Chen *et al*. 2001) of an intelligent structure (plate or shell structure) is

$$\boldsymbol{M}\ddot{\delta} + \boldsymbol{C}\dot{\delta} + \boldsymbol{K}\delta = \boldsymbol{D}\boldsymbol{U} \tag{1}$$

Where $\boldsymbol{M}$ is the mass matrix; $\boldsymbol{C}$ is the damping matrix; $\boldsymbol{K}$ is the stiffness matrix; $D_{n\times r}$ is control matrix, which is determined by the position of actuators; δ is the nodal displacement vector; $U_{r\times 1}$ is control vector; r is DOF's (degree of freedom) number of nodes which are relative with actuators, n is structural DOF's number. Let the state vector be as

$$\boldsymbol{X} = \begin{Bmatrix} \delta \\ \dot{\delta} \end{Bmatrix} \tag{2}$$

So that the state equation can be expressed as

$$\dot{\boldsymbol{X}} = \boldsymbol{A}\boldsymbol{X} + \boldsymbol{B}\boldsymbol{U} \tag{3}$$

$$\boldsymbol{X}(t_0) = \boldsymbol{X}_0 \tag{4}$$

Where

$$\boldsymbol{A} = \begin{bmatrix} \boldsymbol{O}_{n\times n} & \boldsymbol{I}_{n\times n} \\ -\boldsymbol{M}^{-1}\boldsymbol{K} & -\boldsymbol{M}^{-1}\boldsymbol{C} \end{bmatrix}_{2n\times 2n} \tag{5}$$

$$\boldsymbol{B} = \begin{bmatrix} \boldsymbol{O}_{n\times r} \\ \boldsymbol{M}^{-1}\boldsymbol{D} \end{bmatrix}_{2n\times r} \tag{6}$$

Where $O_{n\times n}$ is zero matrix; $I_{n\times n}$ is identity matrix.

The object is to determine an optimal shape control minimizing the quadratic performance measure

$$J = \frac{1}{2}\boldsymbol{X}^T(t_f)\boldsymbol{Q}_3\boldsymbol{X}(t_f) + \frac{1}{2}\int_{t_0}^{t_f}[\boldsymbol{X}^T(t)\boldsymbol{Q}_1(t)\boldsymbol{X}(t) + \boldsymbol{U}^T\boldsymbol{Q}_2(t)\boldsymbol{U}]dt \tag{7}$$

Where $\boldsymbol{Q}_1$, $\boldsymbol{Q}_3$ are real symmetric positive semi-definite matrices and $\boldsymbol{Q}_2$ is a real symmetric positive definite matrix; Item U^TQ_2U is of effect limiting control amplitude; Item $X^T(t_f)Q_3X(t_f)$ is limiting the final control precision of the structure; t_f is final time of control. The optimal shape control problem using the performance measure Eq. (7) can be interpreted as the problem of driving the initial state as close as possible to zero while placing a penalty on the control effort, i.e., displacements are as close as possible to zero, therefore, the structure keeps the original shape.

By the Hamilton's necessary condition for optimality, the optimal shape control can be obtained (Meirovitch 1990)

$$\boldsymbol{U}^*(t) = -\boldsymbol{Q}_2^{-1}\boldsymbol{B}^T\boldsymbol{P}\boldsymbol{X} \tag{8}$$

Where $G(t) = Q_2^{-1}B^TP$ is the optimal feedback control gain matrix; Matrix P satisfies the Riccati equation

$$\dot{\boldsymbol{P}} = -\boldsymbol{P}\boldsymbol{A} - \boldsymbol{A}^T\boldsymbol{P} - \boldsymbol{Q}_1 + \boldsymbol{P}\boldsymbol{B}\boldsymbol{Q}_2^{-1}\boldsymbol{B}^T\boldsymbol{P}^T \tag{9}$$

$$\boldsymbol{P}(t_f) = \boldsymbol{Q}_3 \tag{10}$$

From Eq. (9), the Riccati matrix $\boldsymbol{P}$ is symmetric, and Kalman proved that $\boldsymbol{P}$ is constant as $t \to \infty$.

3. The block iterative algorithm

Virtually, the optimal control U^* can be expressed as the sum of the displacement negative feedback and velocity negative feedback

$$\boldsymbol{U}^* = (C_1^* \quad C_2^*)\boldsymbol{X} = \boldsymbol{C}_1^*\delta + \boldsymbol{C}_2^*\dot{\delta} \tag{11}$$

Letting

$$\boldsymbol{P} = \begin{bmatrix} \boldsymbol{P}_{11} & \boldsymbol{P}_{12} \\ \boldsymbol{P}_{21} & \boldsymbol{P}_{22} \end{bmatrix} \tag{12}$$

Where

$$\boldsymbol{P}_{11}^T = \boldsymbol{P}_{11}, \quad \boldsymbol{P}_{21}^T = \boldsymbol{P}_{12}, \quad \boldsymbol{P}_{22}^T = \boldsymbol{P}_{22} \tag{13}$$

Inserting Eqs.(2), (6), (11) and (12) to Eq. (8) yields

$$-\boldsymbol{Q}_2^{-1}(\boldsymbol{O} \quad \boldsymbol{M}^{-1}\boldsymbol{D})\begin{bmatrix}\boldsymbol{P}_{11} & \boldsymbol{P}_{12}\\ \boldsymbol{P}_{21} & \boldsymbol{P}_{22}\end{bmatrix}\begin{bmatrix}\delta\\ \dot{\delta}\end{bmatrix} = (\boldsymbol{C}_1^* \quad \boldsymbol{C}_2^*)\begin{bmatrix}\delta\\ \dot{\delta}\end{bmatrix}$$

$$-\boldsymbol{Q}_2^{-1}(\boldsymbol{M}^{-1}\boldsymbol{D}\boldsymbol{P}_{21} \quad \boldsymbol{M}^{-1}\boldsymbol{D}\boldsymbol{P}_{22})\begin{bmatrix}\delta\\ \dot{\delta}\end{bmatrix} = \boldsymbol{C}_1^*\delta + \boldsymbol{C}_2^*\dot{\delta}$$

Simplifying

$$\boldsymbol{C}_1^* = -\boldsymbol{Q}_2^{-1}\boldsymbol{M}^{-1}\boldsymbol{D}\boldsymbol{P}_{21} \tag{14}$$

$$\boldsymbol{C}_2^* = -\boldsymbol{Q}_2^{-1}\boldsymbol{M}^{-1}\boldsymbol{D}\boldsymbol{P}_{22} \tag{15}$$

Where $\boldsymbol{C}_1^*$ is the displacement negative feedback gain matrix; $\boldsymbol{C}_2^*$ is the velocity negative feedback gain matrix.

If the solution matrices $\boldsymbol{P}_{21}$, $\boldsymbol{P}_{22}$ is obtained, the optimal control $\boldsymbol{U}^*$ can be computed by Eqs. (8), (14) and (15). Letting

$$\boldsymbol{Q}_1 = \begin{bmatrix}\boldsymbol{Q}_{11}^1 & \boldsymbol{Q}_{12}^1\\ \boldsymbol{Q}_{21}^1 & \boldsymbol{Q}_{22}^1\end{bmatrix}, \quad \boldsymbol{Q}_3 = \begin{bmatrix}\boldsymbol{Q}_{11}^3 & \boldsymbol{Q}_{12}^3\\ \boldsymbol{Q}_{21}^3 & \boldsymbol{Q}_{22}^3\end{bmatrix} \tag{16}$$

Inserting Eqs. (5), (6), (12) and (16) to Eq. (9) yields

$$\begin{bmatrix}\dot{\boldsymbol{P}}_{11} & \dot{\boldsymbol{P}}_{12}\\ \dot{\boldsymbol{P}}_{21} & \dot{\boldsymbol{P}}_{22}\end{bmatrix} = -\begin{bmatrix}\boldsymbol{P}_{11} & \boldsymbol{P}_{12}\\ \boldsymbol{P}_{21} & \boldsymbol{P}_{22}\end{bmatrix}\begin{bmatrix}\boldsymbol{O} & \boldsymbol{I}\\ -\boldsymbol{M}^{-1}\boldsymbol{K} & -\boldsymbol{M}^{-1}\boldsymbol{C}\end{bmatrix} -$$

$$-\begin{bmatrix}\boldsymbol{O} & -\boldsymbol{K}\boldsymbol{M}^{-1}\\ \boldsymbol{I} & -\boldsymbol{C}^T\boldsymbol{M}^{-1}\end{bmatrix}\begin{bmatrix}\boldsymbol{P}_{11} & \boldsymbol{P}_{12}\\ \boldsymbol{P}_{21} & \boldsymbol{P}_{22}\end{bmatrix} - \begin{bmatrix}\boldsymbol{Q}_{11}^1 & \boldsymbol{Q}_{12}^1\\ \boldsymbol{Q}_{21}^1 & \boldsymbol{Q}_{22}^1\end{bmatrix} +$$

$$+\begin{bmatrix}\boldsymbol{P}_{11} & \boldsymbol{P}_{12}\\ \boldsymbol{P}_{21} & \boldsymbol{P}_{22}\end{bmatrix}\begin{bmatrix}\boldsymbol{O} & \boldsymbol{O}\\ \boldsymbol{O} & \boldsymbol{M}^{-1}\boldsymbol{D}\boldsymbol{Q}_2^{-1}\boldsymbol{M}^{-1}\boldsymbol{D}^{\boldsymbol{T}}\end{bmatrix}\begin{bmatrix}\boldsymbol{P}_{11} & \boldsymbol{P}_{12}\\ \boldsymbol{P}_{21} & \boldsymbol{P}_{22}\end{bmatrix}^T$$

simplifying

$$\dot{\boldsymbol{P}}_{11} = (\boldsymbol{K}\boldsymbol{M}^{-1}\boldsymbol{P}_{21})^T + \boldsymbol{K}\boldsymbol{M}^{-1}\boldsymbol{P}_{21} - \boldsymbol{Q}_{11}^1 + (\boldsymbol{D}^T\boldsymbol{M}^{-1}\boldsymbol{P}_{21})^T\boldsymbol{Q}_2^{-1}(\boldsymbol{D}^T\boldsymbol{M}^{-1}\boldsymbol{P}_{21}) \tag{17}$$

$$\dot{\boldsymbol{P}}_{21} = (\boldsymbol{K}\boldsymbol{M}^{-1}\boldsymbol{P}_{22})^T + \boldsymbol{C}^T\boldsymbol{M}^{-1}\boldsymbol{P}_{21} - \boldsymbol{P}_{11} - \boldsymbol{Q}_{21}^1 + (\boldsymbol{D}^T\boldsymbol{M}^{-1}\boldsymbol{P}_{22})^T\boldsymbol{Q}_2^{-1}(\boldsymbol{D}^T\boldsymbol{M}^{-1}\boldsymbol{P}_{21}) \tag{18}$$

$$\dot{\boldsymbol{P}}_{22} = (\boldsymbol{C}^T\boldsymbol{M}^{-1}\boldsymbol{P}_{22})^T + \boldsymbol{C}^T\boldsymbol{M}^{-1}\boldsymbol{P}_{22} - \boldsymbol{P}_{21} - \boldsymbol{P}_{21}^T - \boldsymbol{Q}_{22}^1 + (\boldsymbol{D}^T\boldsymbol{M}^{-1}\boldsymbol{P}_{22})^T\boldsymbol{Q}_2^{-1}(\boldsymbol{D}^T\boldsymbol{M}^{-1}\boldsymbol{P}_{22}) \tag{19}$$

$$\boldsymbol{P}_{11}(t_f) = \boldsymbol{Q}_{11}^3, \quad \boldsymbol{P}_{21}(t_f) = \boldsymbol{Q}_{21}^3, \quad \boldsymbol{P}_{22}(t_f) = \boldsymbol{Q}_{22}^3 \tag{20}$$

Which can be integrated backward in time by the initial conditions. For Eqs. (9) and (10), the four-order Runge-Kutta formulation is as

$$\begin{cases} \boldsymbol{W}_1 = f(\boldsymbol{P}_i) \\ \boldsymbol{W}_2 = f\left(\boldsymbol{P}_i + \dfrac{\boldsymbol{h}}{2}\boldsymbol{W}_1\right) \\ \boldsymbol{W}_3 = f\left(\boldsymbol{P}_i + \dfrac{\boldsymbol{h}}{2}\boldsymbol{W}_2\right) \\ \boldsymbol{W}_4 = f(\boldsymbol{P}_i + \boldsymbol{h}\boldsymbol{W}_3) \\ \boldsymbol{p}_{i+1} = \boldsymbol{P}_i + \dfrac{\boldsymbol{h}}{6}(\boldsymbol{W}_1 + 2\boldsymbol{W}_2 + 2\boldsymbol{W}_3 + \boldsymbol{W}_4) \end{cases} \tag{21}$$

Where

$$f(\boldsymbol{P}) = -\boldsymbol{P}\boldsymbol{A} - \boldsymbol{A}^T\boldsymbol{P} - \boldsymbol{Q}_1 + \boldsymbol{P}\boldsymbol{B}\boldsymbol{Q}_2^{-1}\boldsymbol{B}^T\boldsymbol{P}^T \tag{22}$$

h is step length. For the structural stiffness matrix (Meirovitch 1990), if

$$10^{I-1} \le \max_{1 \le \boldsymbol{i} \le \mathbf{n}} \{|\boldsymbol{k}_{ii}|\} \le 10^I \tag{23}$$

The present algorithm is convergent as h is less than 10^{-I} and divergent as h is more than 10^{-I+1}. For the sake of computation, let h be equals to 10^{-I}. Using Eq. (21) and solving Eqs. (17), (18) and (19) simultaneously, we can obtain $\boldsymbol{P}_{21}$, $\boldsymbol{P}_{22}$. The above method is very well for saving memory and computing time.

4. Modal control algorithm

The deformation of the structure is caused mainly by the response of the lower modes, and the amplitude responses of higher modes are very small in contrast to the lower modes. So that lower modes play main role in the deformation of the structure.

Because the shape control requests the real-time control, the computing time of the feedback control should be as short as possible and the computing precision be also reasonable. For this reason, the modal control algorithm is presented.

By using expansion theorem, we obtain

$$\{\delta\} = \sum_{\boldsymbol{i}=1}^{\boldsymbol{n}_f} \boldsymbol{\phi}_i \boldsymbol{q}_i = [\Phi]\{\boldsymbol{q}\} \tag{24}$$

Where $\boldsymbol{q}_i (i = 1, 2, \ldots, n_f)$ is modal coordinate and $\{\boldsymbol{q}\}$ is the corresponding modal coordinate vector; $[\Phi]$ is the modal matrix; n_f is the number of modes we used; $\boldsymbol{\phi}_i$ $(i = 1, 2, \ldots, n_f)$ satisfies the normalizing condition, i.e.,

$$[\Phi]^T[\boldsymbol{M}][\Phi] = [\boldsymbol{I}] \qquad [\Phi]^T[\boldsymbol{K}][\Phi] = [\Omega^2] \tag{25}$$

Where $[\Omega^2]$ is the diagonal matrix of eigenvalues, i.e.,

$$[\Omega^2] = \boldsymbol{diag}[\omega_1^2, \omega_2^2, \ldots, \omega_{n_f}^2] \tag{26}$$

Substituting Eq. (24) into Eq. (1) and pre-multiplying it by $[\Phi]^T$, we have

$$\{\ddot{\boldsymbol{q}}\} + 2[\xi][\Omega]\{\dot{\boldsymbol{q}}\} + [\Omega^2]\{\boldsymbol{q}\} = [\Phi]^T[\boldsymbol{D}]\{\boldsymbol{u}\} = \boldsymbol{f}_{mc} \tag{27}$$

Where $[\xi] = \boldsymbol{diag}[\xi_1, \xi_2, \ldots, \xi_{nf}]$ is the diagonal matrix of the structural damping; $\boldsymbol{f}_{mc}$ is modal control force.

The state equation in the modal coordinates is obtained

$$\dot{\boldsymbol{Y}} = \boldsymbol{A}_0\boldsymbol{Y} + \boldsymbol{B}_0\boldsymbol{f}_{mc} \tag{28}$$

$$\boldsymbol{Y}(\boldsymbol{t}_0) = \boldsymbol{Y}_0 \tag{29}$$

Where

$$\boldsymbol{Y} = \begin{Bmatrix} \boldsymbol{q} \\ \dot{\boldsymbol{q}} \end{Bmatrix}, \quad \boldsymbol{A}_0 = \begin{bmatrix} \boldsymbol{O} & \boldsymbol{I} \\ -[\Omega^2] & -2[\xi][\Omega] \end{bmatrix}, \quad \boldsymbol{B}_0 = \begin{bmatrix} \boldsymbol{O} \\ \boldsymbol{I} \end{bmatrix} \tag{30}$$

Here the performance measure is

$$\boldsymbol{J} = \frac{1}{2}\boldsymbol{Y}^{\boldsymbol{T}}(\boldsymbol{t}_f)\boldsymbol{Q}_{30}\boldsymbol{Y}(\boldsymbol{t}_f) + \frac{1}{2}\int_{t_0}^{t_f}[\boldsymbol{Y}^{\boldsymbol{T}}(\boldsymbol{t})\boldsymbol{Q}_{10}\boldsymbol{Y}(\boldsymbol{t}) + \boldsymbol{f}_{mc}^{\boldsymbol{T}}(\boldsymbol{t})\boldsymbol{Q}_{20}\boldsymbol{f}_{mc}(\boldsymbol{t})]\boldsymbol{dt} \tag{31}$$

The optimal modal control is

$$\boldsymbol{f}_{mc}^{*} = -\boldsymbol{Q}_{20}^{-1}\boldsymbol{B}_0^T\overline{\boldsymbol{P}}\boldsymbol{Y} \tag{32}$$

Where $\boldsymbol{G}_0(\boldsymbol{t}) = \boldsymbol{Q}_{20}^{-1}\boldsymbol{B}_0^T\overline{\boldsymbol{P}}$ is the optimal modal feedback gain matrix, matrix $\overline{\boldsymbol{P}}$ satisfies Riccati equation.

$$\dot{\overline{\boldsymbol{P}}} = -\overline{\boldsymbol{P}}\boldsymbol{A}_0 - \boldsymbol{A}_0^T\overline{\boldsymbol{P}} - \boldsymbol{Q}_{10} + \overline{\boldsymbol{P}}\boldsymbol{B}_0\boldsymbol{Q}_{20}^{-1}\boldsymbol{B}_0^T\overline{\boldsymbol{P}}^T \tag{33}$$

By using the block iterative algorithm in section 3, we can obtain matrix $\overline{\boldsymbol{P}}$, and the optimal modal control can be obtained.

5. Numerical example

In this section, the dynamic characteristics of a shell structure (Fig. 1) with surface coupled distributed piezoelectric sensor and actuator are evaluated. The first nine mode shapes and associated voltage distributions are obtained.

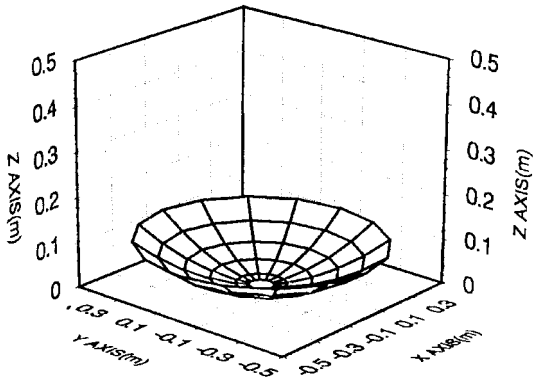

Fig. 1 Finite element modeling of a shell structure with distributed piezoelectric sensor/actuator

5.1 Model definition

The shell structure (diameter: 1 m; thickness: 5 mm; height: 100 mm; ρ = 2.68E3; E = 8.0E9; μ = 0.28) with a distributed piezoelectric PVDF (material property can be found in Tzou *et al*. 1990) layer (0.1 mm) serving as a distributed actuator on the top surface, and another PVDF on the bottom surface as a distributed sensor, was used as a numerical example. The structure was divided into 240 elements, 80 for each layer.

5.2 Mode shape and modal voltage distribution

The output signals of each node on the distributed piezoelectric sensor layer can be calculated as a function of the displacements (see Eq. (67) in Chen *et al*. 2001). After the nodal voltage is calculated, the overall voltage distribution of the structure can be plotted by connecting all nodal voltage amplitudes. Thus, for a given mode, the modal voltage distribution can be observed. The first nine structural mode shapes and modal voltage distributions are illustrated in Figs. 2-10, here, the first and second mode, the third and fourth, the fifth and sixth, the eighth and ninth are repeated frequencies respectively.

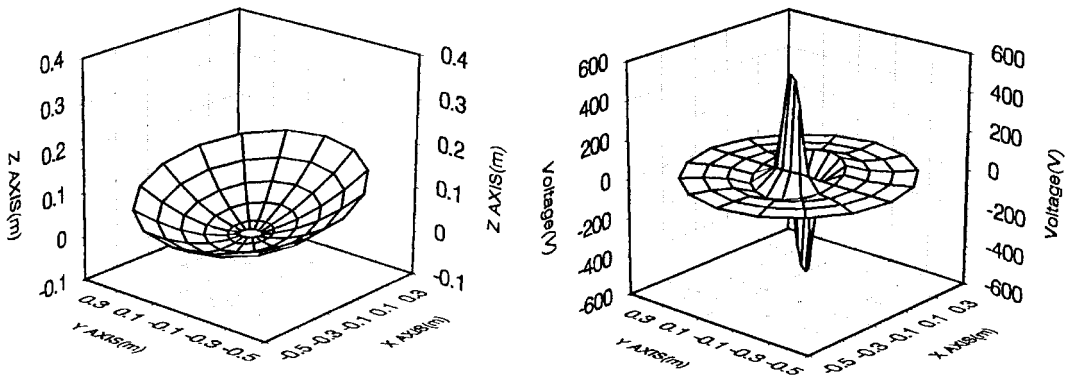

Fig. 2 First mode shape and modal voltage distribution

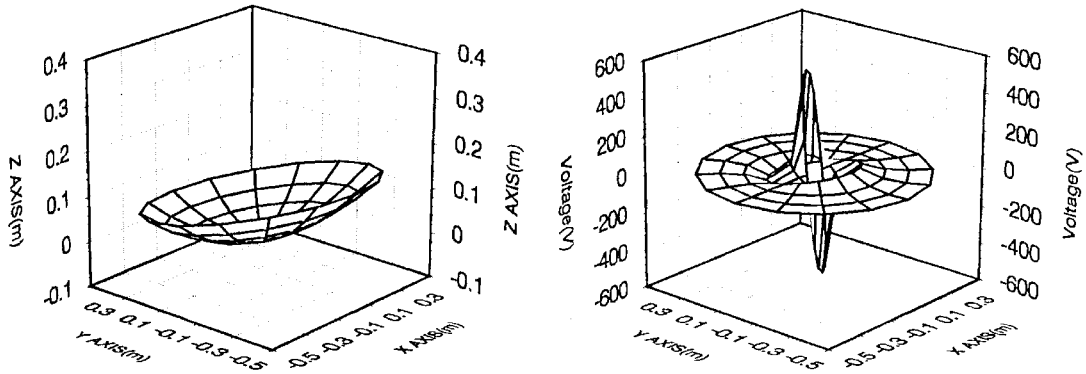

Fig. 3 Second mode shape and modal voltage distribution

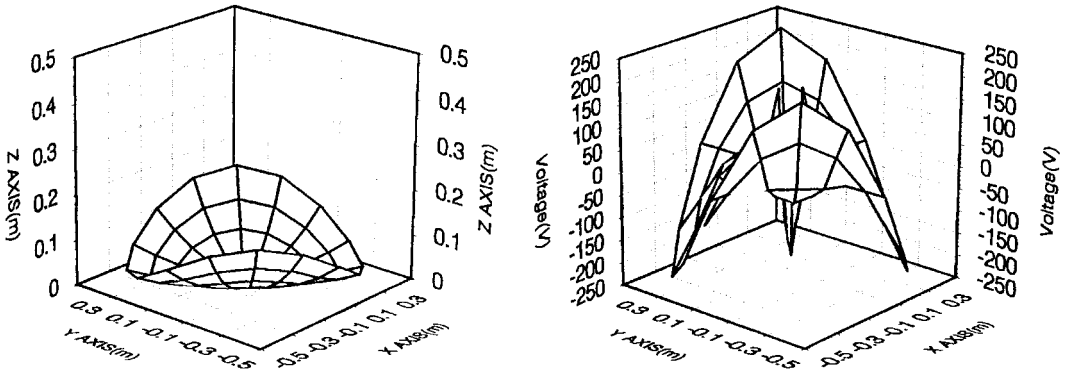

Fig. 4 Third mode shape and modal voltage distribution

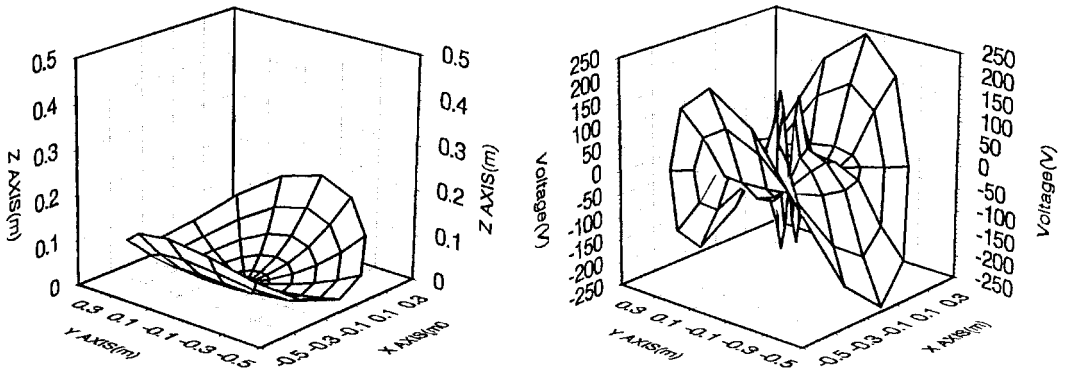

Fig. 5 Fourth mode shape and modal voltage distribution

The first mode is vibration along the positive direction of x-axis; the second mode along y-axis; the third mode along the lines of the slope angle $\frac{\pi}{4}$ and $\frac{3}{2}\pi$; the fourth mode along X-axis and negative X-axis, and so on, but the seventh modal is vertical up or down vibration. From Figs. 2-10, the deformation of the structure is mainly caused by the lower modes. It plays an important role in the structural deformation.

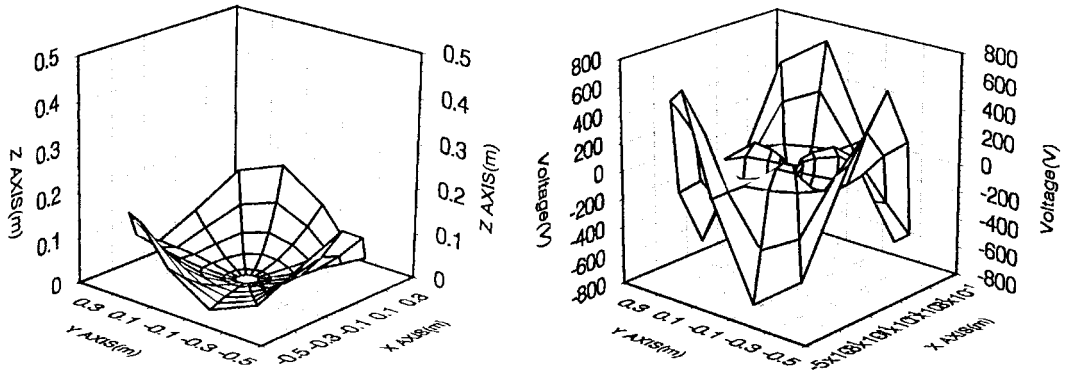

Fig. 6 Fifth mode shape and modal voltage distribution

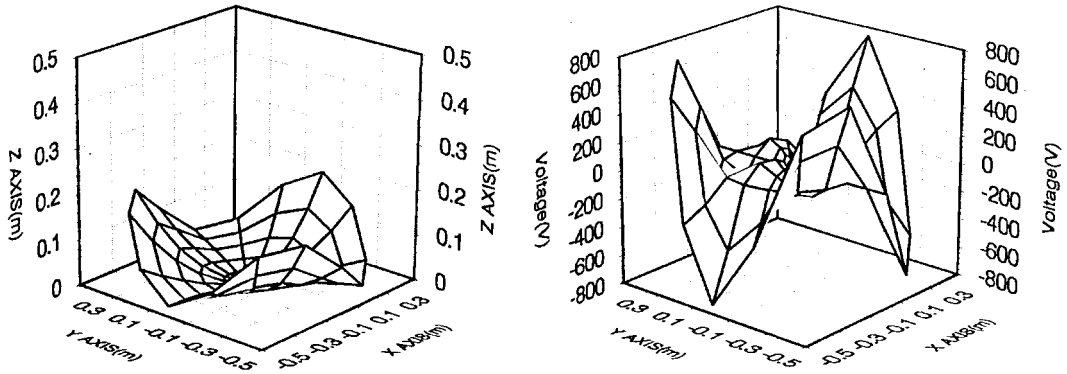

Fig. 7 Sixth mode shape and modal voltage distribution

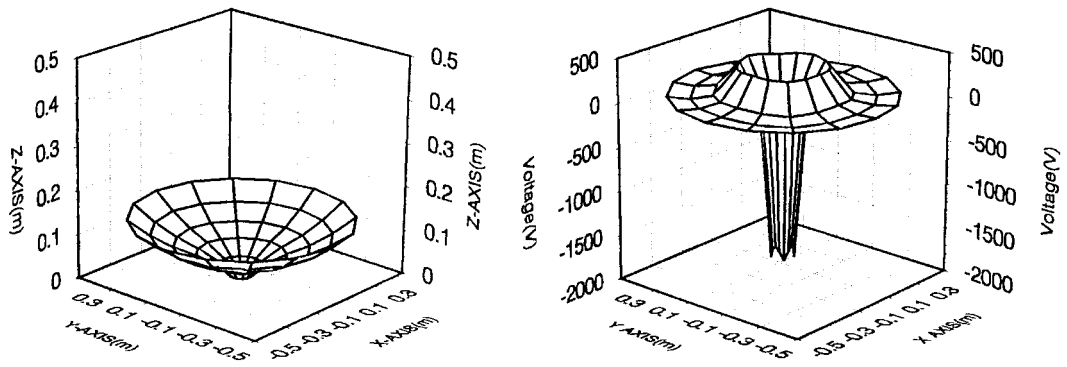

Fig. 8 Seventh mode shape and modal voltage distribution

5.3 The optimal shape control

Letting $\boldsymbol{Q}_1$ and $\boldsymbol{Q}_2$ are equal to identity matrix I respectively, $\boldsymbol{Q}_3$ is zero matrix; C is damping matrix (here, $\alpha = 0.0121$, $\beta = 8.2270 \times 10^{-5}$); D is equal to identity matrix I. When a pulse force is applied at edge nodes of the structure, the z-displacement of the edge node is plotted in Fig. 11. By

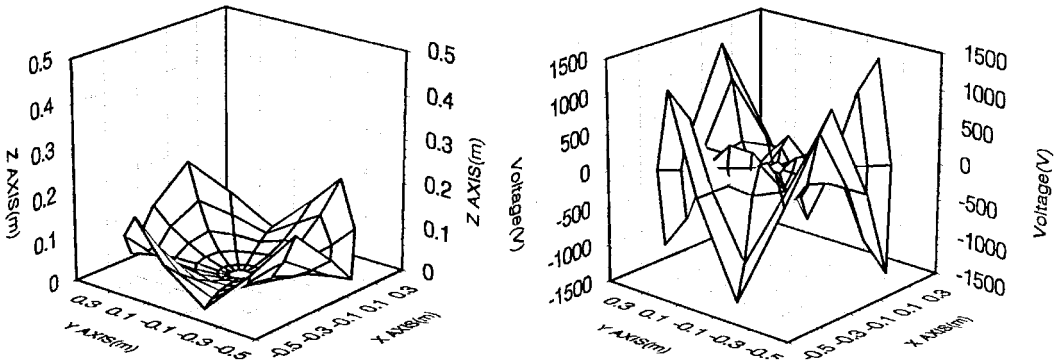

Fig. 9 Eighth mode shape and modal voltage distribution

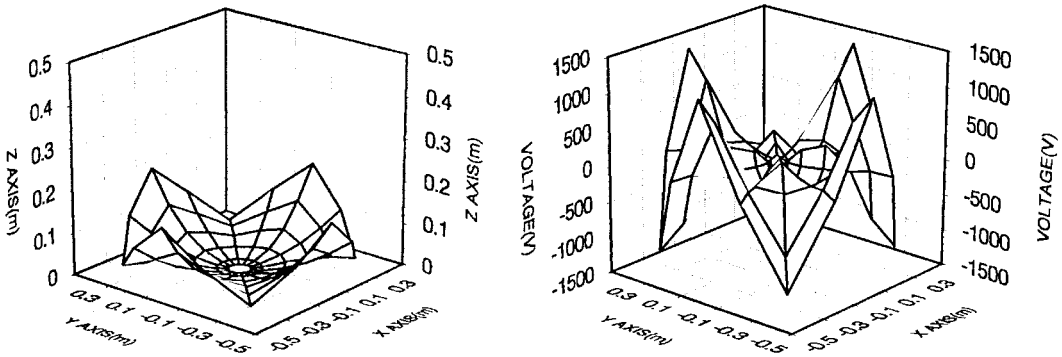

Fig. 10 Ninth mode shape and modal voltage distribution

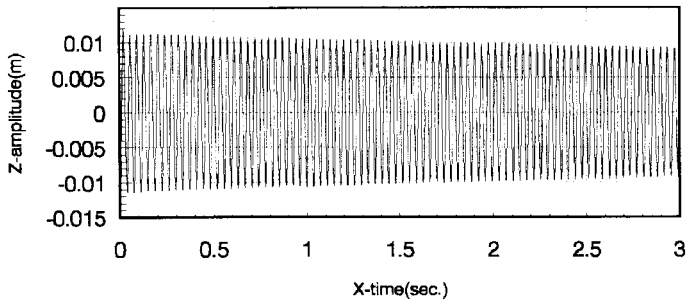

Fig. 11 The pulse response of the antenna structure

adding the optimal shape control to the structure (section 3), the *z*-displacement of the same node is plotted in Fig. 12. In computing the optimal shape control, the block iterative algorithm is used. For the higher order structure, the other methods aren't available, the main reason is because they cannot guarantee the real-time control; by adding the optimal modal shape control to the structure (section 4, let $n_f = 9$), the *z*-displacement of the same node is plotted in Fig. 13.

From the above Figs. 11-13, the original shape of the antenna structure can be recovered quickly,

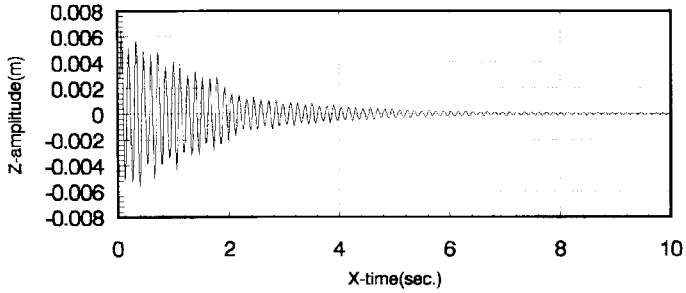

Fig. 12 The optimal shape control of the antenna structure

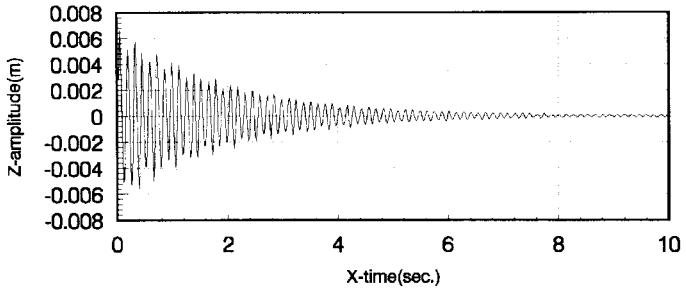

Fig. 13 The optimal modal shape control of the antenna structure

and the effect of the optimal modal shape control is almost the same as the one of the optimal shape control for all state, but the CPU time is about 1 minute, and the all state is about 55 minutes (computing with common Pentium III PC), so that the optimal modal shape control algorithm is favorable. Adjusting the coefficient matrix of the performance measure, we can obtain the different control effects.

6. Conclusions

From the numerical example, the modal control algorithm is effective. It needs shorter time to obtain the optimal control. If the method of section 3 is used to calculate the optimal shape control of all state feedback, it needs the more computing time to compute the gain matrix for the large structure and cannot reach the effects of the real-time control, but the two methods combined will result in the good effects. Therefore, the modal control algorithm is very important for the real-time control.

Acknowledgements

This project was supported by the National Natural Science Foundation and Mechanical Technology development Foundation of China. The authors are grateful to reviewers for their helpful suggestions and discussions.

References

Ahmad, S., Irons, B.M. and Zienkiewicz, O.C. (1970), "Analysis of thick and thin shell structure by curved elements", *Int. J. Numer. Meth. Eng.*, **2**, 419-451.

Atluri, S.N. and Amos, A.K. (1988), *Large Space Structures: Dynamics and Control*, Springer-Verlag, Berlin.

Guyan, R.J. (1965), "Reduction of stiffness and mass matrices", *AIAA J.*, **3**(2), 380-386.

Hwang, W.S. and Park, H.C. (1993), "Finite element modeling of piezoelectric sensors and actuators", *AIAA J.*, **31**(5).

Im, S. and Atluri, S.N. (1989), "Effects of a piezo-actuator on a finitely deformed beam subjected to general loading", *AIAA J.*, **27**(12), 1801-1807.

Meirovitch, L. (1990), *Dynamics and Control of Structures*, Wiley, New York.

Pawsey, S.F. and Clough, R.W. (1971), "Improved numerical integration of thick slab finite elements", *Int. J. Numer. Meth. Eng.*, **3**, 575-586.

Shi, G. and Atluri, S.N. (1990), "Active control of nonlinear dynamic response of space-frames using piezo-electric actuators", *Comput. Struct.*, **34**(4), 549- 564.

Suhuan, Chen, and Guofeng, Yao (2001), "A new piezoelectric shell element and its application in static shape control", *Struct. Eng. Mech.*, **12**(5), 491-506.

Tzou, H.S. and Tseng, C.I. (1990), "Distributed piezoelectric sensor/actuator design for dynamic measurement/ control of distributed parameter systems: a piezoelectric finite element approach", *J. Sound Vib.*, **138**(1), 17-34.

Xie, Y.Q. and He, F.B. (1981), *A Finite Element Method in Elastic and Plastic Mechanics*, Machine Industry Press, China.

Zhang, J.D., O'Donoghue, P.D. and Atluri, S.N. (1986), "Analysis and control of finite deformations of plates and shells", Chapter 6 in *Finite Element Methods for Plate and Shell Structure*, (Eds: T.T.R. Hughes and E. Hinton), Pineridge Press, Swansea, 127-153.

Zienkiewicz, O.C., Too, T. and Taylor, R.L. (1971), "Reduced integration technique in general analysis of plates and shells", *Int. J. Numer. Meth. Eng.*, **3**, 275-290.